Surface Stabilized Nanosized Ce$_x$Zr$_{1-x}$O$_2$ Solid Solutions over SiO$_2$: Characterization by XRD, Raman, and HREM Techniques[†]

Benjaram M. Reddy,* Pandian Lakshmanan, and Ataullah Khan

Inorganic and Physical Chemistry Division, Indian Institute of Chemical Technology,
Hyderabad 500 007, India

Stéphane Loridant

Institut de Recherches sur la Catalyse- CNRS, 2 Avenue A. Einstein, 69626 Villeurbanne Cedex, France

Carlos López-Cartes, Teresa C. Rojas, and Asunción Fernández

Instituto de Ciencia de Materiales de Sevilla (CSIC-UNSE), Avda. Américo Vespucio no. 49,
41092 Sevilla, Spain

Received: March 19, 2005; In Final Form: May 13, 2005

Ce$_x$Zr$_{1-x}$O$_2$ solid solutions deposited over silica surface were investigated by X-ray diffraction (XRD), Raman spectroscopy (RS), and high-resolution transmission electron microscopy (HREM) techniques in order to understand the role of silica support and the temperature stability of these composite oxides. For the purpose of comparison, an unsupported Ce$_x$Zr$_{1-x}$O$_2$ was also synthesized and subjected to characterization by various techniques. The Ce$_x$Zr$_{1-x}$O$_2$/SiO$_2$ (CZ/S) (1:1:2 mole ratio based on oxides) was synthesized by depositing Ce$_x$Zr$_{1-x}$O$_2$ solid solution over a colloidal SiO$_2$ support by a deposition precipitation method and unsupported Ce$_x$Zr$_{1-x}$O$_2$ (CZ) (1:1 mole ratio based on oxides) was prepared by a coprecipitation procedure, and the obtained catalysts were subjected to thermal treatments from 773 to 1073 K. The XRD measurements disclose the presence of cubic phases with the composition Ce$_{0.75}$Zr$_{0.25}$O$_2$ and Ce$_{0.6}$Zr$_{0.4}$O$_2$ in CZ samples, while CZ/S samples possess Ce$_{0.75}$Zr$_{0.25}$O$_2$, Ce$_{0.6}$Zr$_{0.4}$O$_2$, and Ce$_{0.5}$Zr$_{0.5}$O$_2$ in different proportions. The crystallinity of these phases increased with increasing calcination temperature. The cell a parameter estimations indicate contraction of ceria lattice due to the incorporation of zirconium cations into the CeO$_2$ unit cell. Raman measurements indicate the presence of oxygen vacancies, lattice defects, and displacement of oxygen ions from their normal lattice positions in both the series of samples. The HREM results reveal, in the case of CZ/S samples, a well-dispersed nanosized Ce−Zr-oxides over the surface of amorphous SiO$_2$. The structural features of these crystals as determined by digital diffraction analysis of experimental images reveal that the Ce−Zr−oxides are mainly in the cubic geometry and exhibit high thermal stability. Oxygen storage capacity measurements by a thermogravimetric method reveal a substantial enhancement in the oxygen vacancy concentration of CZ/S sample over the unsupported CZ sample.

Introduction

Among various mixed oxides based on cerium oxide, ceria−zirconia has attracted much attention and emerged as a powerful combination due to its tremendous technological implications.[1] The versatile applicability originates primarily because of their superior catalytic properties resulting from the combination of oxygen storage characteristics (OSC) of cerium oxide and highly refractory properties of zirconium oxide.[1,2] Taken in different stoichiometries, the unsupported and supported forms of the Ce$_{1-x}$Zr$_x$O$_2$ solid solutions have been employed for a variety of industrially important reactions which include three-way catalysis,[3−5] CO oxidation,[6] partial oxidation of CH$_4$ to syngas,[7] CO$_2$ reforming of CH$_4$,[8] catalytic combustion of hydrocarbons,[9] methanol decomposition to syn-gas,[10] steam reforming of ethanol,[11] and so on. It is now well established that nanophasic Ce$_{1-x}$Zr$_x$O$_2$ exhibits excellent catalytic activity for

processes such as dehydration of alcohols,[12] catalytic oxidation of methane,[13,14] and CO oxidation.[15,16] Very recently, Pt/Ce$_x$Zr$_{1-x}$O$_2$/Al$_2$O$_3$[17] and CuO−CeO$_2$−ZrO$_2$[18,19] systems have also been investigated for preferential oxidation of CO in the presence of H$_2$, and H$_2$ rich steam reformates, respectively. The Ce$_x$Zr$_{1-x}$O$_2$ also promotes processes related to hydrogen production such as hydrocarbon reforming and partial oxidation.[20−22] The technological applicability of Ce$_x$Zr$_{1-x}$O$_2$ is expanding very rapidly.[1]

Relative to ceria, ceria−zirconia mixed oxides show slightly better redox properties and better thermal stability.[1,22] Despite this, these unsupported oxides are susceptible to a fall in the surface area and a decrease in the stability of the structure during high-temperature applications.[23,24] While one can find numerous reports in the literature on the preparation and characterization of unsupported forms of Ce$_{1-x}$Zr$_x$O$_2$,[1] only few studies have been focused on the supported Ce$_{1-x}$Zr$_x$O$_2$ systems.[25,26] The design of nanocomposites where the Ce$_x$Zr$_{1-x}$O$_2$ phase is dispersed over a stable support could represent a suitable way to improve thermal and structural stability of these systems. A

highly dispersed nanosized CeO_2 over SiO_2 has already revealed improved surface area, better thermal resistance and a high oxygen storage capacity, which are essential for a successful catalyst.[27] To date, relatively few papers have been devoted to this topic and only recently the effects of addition of alumina on the thermal stability and reduction behavior of ceria-zirconia mixed oxides have been investigated.[25,26,28] The aim of the present study was to synthesize and characterize silica supported $Ce_{1-x}Zr_xO_2$ ($x \geq 0.5$) nanosized oxides with improved physical properties such as high specific surface area, smaller particle size, and better resistance toward thermal sintering. Silica is one of the most widely available supports with excellent chemical resistance, thermal stability, and high specific surface area, which enhances a high dispersion and catalytic activity of the dispersed active oxides. In this investigation, silica supported high surface area cubic ceria-zirconia nanocomposite oxides were synthesized for the first time by a deposition precipitation method and subjected to various thermal treatments to understand their sintering behavior. For the purpose of comparison, a CeO_2-ZrO_2 sample was also prepared under identical conditions by a coprecipitation method. The physicochemical and structural characterization of various samples was carried out by using X-ray diffraction (XRD), BET surface area, differential thermal analysis (DTA/TGA), Raman spectroscopy, and high-resolution transmission electron microscopy (HREM) techniques. The oxygen storage capacity (OSC) of the mixed oxides was also determined by a thermogravimetry method and correlated with the characterization results.

Experimental Section

Sample Preparation. The CeO_2-ZrO_2 (CZ) composite oxide (1:1 mole ratio based on oxides) was prepared by a coprecipitation method. The CeO_2-ZrO_2/SiO_2 (CZ/S) composite oxide (1:1:2 mole ratio based on oxides) was synthesized by a deposition precipitation method. In a typical experiment, requisite quantities of ammonium cerium(IV) nitrate (Loba Chemie, GR grade) and zirconium(IV) nitrate (Fluka, AR grade) were dissolved separately in deionized water and mixed together. In the later case, the required quantity of colloidal silica (Ludox 40 wt. %, Aldrich, AR grade) was added to aforementioned mixture solution. Dilute aqueous ammonia solution was added dropwise with vigorous stirring until the precipitation was complete (final pH 8.5). The resulting product was filtered off, washed several times with deionized water, oven dried at 383 K for 12 h, and then calcined at 773 K for 5 h in air atmosphere. Portions of the calcined samples were once again heated at 873, 973, and 1073 K for 5 h in a closed muffle furnace in air atmosphere.

X-Ray Diffraction. X-ray powder diffraction patterns were recorded on a Siemens D-5005 diffractometer using a Ni-filtered Cu K_α (0.15418 nm) radiation source. The XRD phases present in the samples were identified with the help of the Powder Diffraction File-International Center for Diffraction Data (PDF-ICDD). The average crystallite size of Ce−Zr−oxide phases was estimated with the help of Debye−Scherrer equation using the XRD data of all prominent lines and the cell *a* parameter was calculated by a standard cubic indexation method using the intensity of the most prominent peak (111).[23,29]

Raman Spectra. The Raman spectra have been achieved on powders at room temperature with a DILOR XY spectrometer equipped with a CCD detector. The emission line at 514.53 nm from an Ar^+ ion laser (Spectra Physics) was focused on the sample under the microscope, the analyzing spot being ~1 μm. The power of the incident beam on the sample was 3 mW. This

TABLE 1: BET Surface Area, fwhm Values, Average Crystallite Size, and 'a′ Cell Parameter Measurements of Cubic $Ce_{1-x}Zr_xO_2$ in CeO_2-ZrO_2 and CeO_2-ZrO_2/SiO_2 Samples Calcined at Different Temperatures

sample	BET SA $(m^2\,g^{-1})$	fwhm[a] $(2\theta°)$	crystallite size[b] (nm)	cell a parameter (Å)
		773 K		
CeO_2-ZrO_2	84	1.55	4.7	5.35
CeO_2-ZrO_2/SiO_2	172	2.80	3.1	5.35
		873 K		
CeO_2-ZrO_2	67	1.54	4.8	5.33
CeO_2-ZrO_2/SiO_2	140	2.54	3.3	5.35
		973 K		
CeO_2-ZrO_2	51	1.50	5.0	5.30
CeO_2-ZrO_2/SiO_2	125	2.30	3.6	5.29
		1073 K		
CeO_2-ZrO_2	36	1.35	5.5	5.27
CeO_2-ZrO_2/SiO_2	112	2.20	3.7	5.26

[a] From most prominent XRD (111) peak. [b] From XRD measurements

power was chosen low enough to avoid laser-heating effects. Time of acquisition was varied according to the intensity of the Raman scattering. The spectral resolution was about 2 cm^{-1}. Homogeneity of the samples was checked focusing the laser beam on various points.

High-Resolution Electron Microscopy. The high-resolution transmission electron microscopy studies were made on Philips CM200 and JEOL 2000EX electron microscopes with 0.23 and 0.21 nm point-to-point resolutions, respectively. For electron microscopy studies, a suspension of the sample in ethanol was placed in an ultrasound bath and then a drop of it was supported on a holey carbon grid. Once the solvent was evaporated, particles that stay on the borders of the holes in the carbon film were studied.

BET Surface Area. The specific surface area of the samples was determined on a Micromeritics Gemini 2360 instrument by N_2 physisorption at liquid N_2 temperature. Before measurements, the samples were oven dried at 393 K for 12 h and flushed in situ with He gas for 2 h.

OSC Measurements. The potential OSC of the samples was examined by oxygen release characteristics of the powders in the temperature range 573−1073 K. The change in the weight of the sample was monitored by thermogravimetry (TG) under cyclic heat treatments in flowing argon or dry air. A commercial Netzsch TG-DTA analyzer (Luxx, STA, 409 PC, Germany) was employed for this purpose. The heat cycle consisted of heating the sample from RT to 1073 K, cooling to 423 K, and again heating to 1073 K without any interruption. All heating and cooling rates were 5 K min^{-1}. The weight loss of the sample during the second heating cycle was used to measure the oxygen release properties (δ). This technique of OSC evaluation is essentially similar to that described previously.[30,31]

Results and Discussion

The N_2 BET surface areas of $Ce_xZr_{1-x}O_2$ (CZ) and Ce_x-$Zr_{1-x}O_2/SiO_2$ (CZ/S) samples calcined at various temperatures are presented in Table 1. The 773 K calcined CZ/S sample exhibits reasonably a high surface area of 172 m^2g^{-1}, while the unsupported CZ sample shows 84 m^2g^{-1}. With increase in calcination temperature from 773 to 1073 K, the specific surface areas of both series of samples decreased considerably. A 35% loss is noted in the case of CZ/S sample, while CZ sample exhibits a 57% loss. The decrease in the surface area with increasing calcination temperature is a general phenomenon due
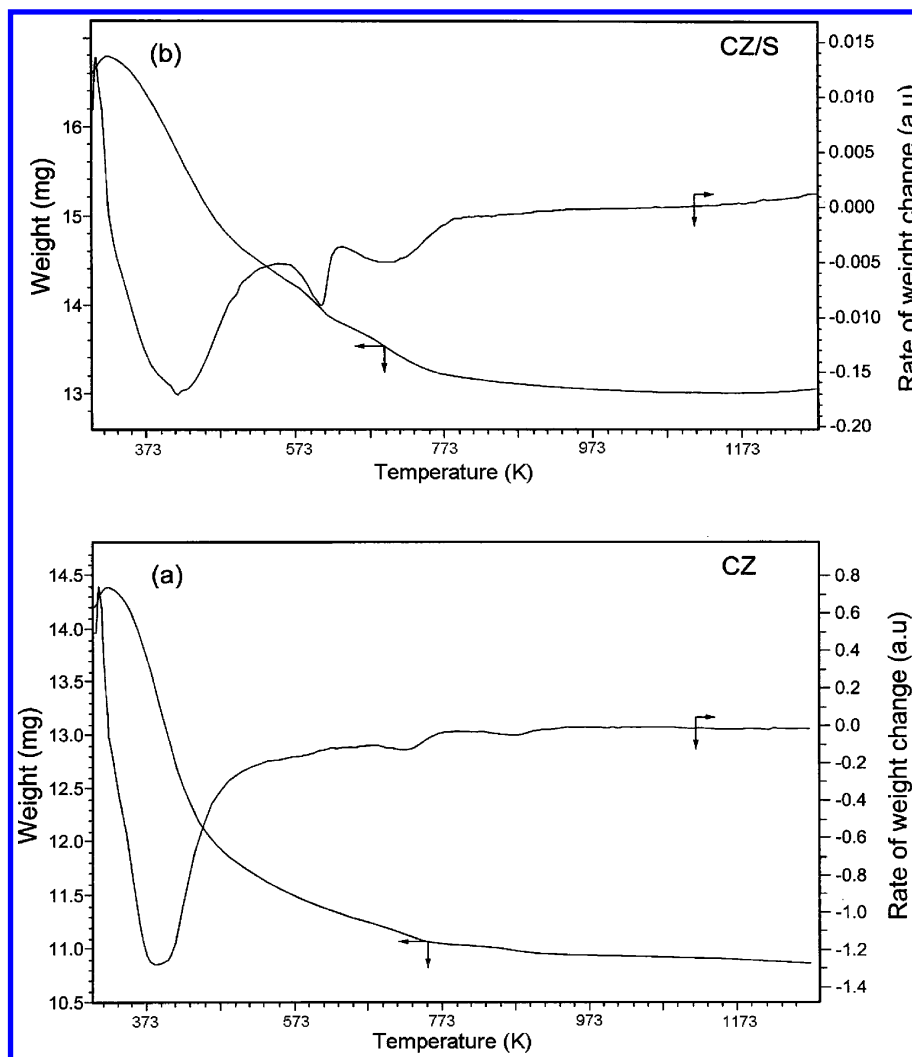
Figure 1. TGA profiles of Ce$_x$Zr$_{1-x}$O$_2$ (CZ) and Ce$_x$Zr$_{1-x}$O$_2$/SiO$_2$ (CZS) uncalcined samples.

to sintering of the samples at high temperatures. It appears from these results that the sintering process is somewhat slow in the case of CZ/S samples. The TG/DTA analysis of these samples before calcination provided some evidence about the role of silica in retarding the decomposition and sintering behavior of Ce$_x$Zr$_{1-x}$O$_2$. As presented in Figure 1, both samples exhibited one major and two minor weight loss peaks. The major low-temperature peak in the range 309−473 K is primarily due to the loss of nondissociative adsorbed water as well as water held on the surface by hydrogen bonding. The minor weight loss peaks at high temperatures are due to loss of water held in the micropores of the gels and dehydroxylation of the surface, respectively. In the case of CZ/S sample, the weight loss from ambient to 625 K is about 16%, and from 625 to 840 K it is 5%. However, the weight loss between 840 and 1273 K is only about 0.5%. It indicates that over the temperature range between 840 and 1273 K, the Ce$_x$Zr$_{1-x}$O$_2$/SiO$_2$ mixed oxide is quite stable in terms of phases and chemical composition. Weight loss of about 23% is observed in the case CZ sample from ambient to 926 K and thereafter a small loss of 0.6% is noted from 926 to 1273 K.

The powder XRD patterns of CZ and CZ/S samples calcined at various temperatures are presented in Figure 2a,b. As can be noted from Figure 2a, the CZ sample calcined at 773 K exhibits poor crystallinity. Only the broad diffraction lines due to a cubic fluorite type phase with the composition Ce$_{0.75}$Zr$_{0.25}$O$_2$ (PDF-ICDD 28-0271) are visible. With increasing calcination tem-

perature, an increase in the intensity and decrease in the width (Table 1, fwhm) of the lines due to better crystallization of this phase could be noted. A slight shift in the peak positions (2θ = 28.86−29.10°) with increasing calcination temperature can be seen which indicate that along with particle growth some compositional changes are also taking place. This effect is primarily due to a progressive increase of zirconium content into the ceria unit cell, since the ionic radius of zirconium (0.84 Å) is smaller than that of cerium cation (0.97 Å).[22] The observed additional broad diffraction patterns at higher calcination temperatures could be assigned to a cubic phase with the composition Ce$_{0.6}$Zr$_{0.4}$O$_2$ (PDF-ICDD 38-1439). Figure 2b represents the diffraction patterns of the CZ/S sample calcined at various temperatures. On the whole the diffraction profiles of CZ/S samples are broader than CZ samples. In the CZ/S case too, a progressive enrichment of zirconium ion into the ceria unit cell could be observed as a function of calcination temperature. The 773 K calcined sample denotes the presence of Ce$_{0.75}$Zr$_{0.25}$O$_2$ phase. With increasing calcination temperature, an increase in the intensity of the lines accompanied by a slight shift in the peak positions (2θ = 28.92 to 29.18 degrees) are clearly observed. Occurrence of Ce$_{0.6}$Zr$_{0.4}$O$_2$ and Ce$_{0.5}$Zr$_{0.5}$O$_2$ (PDF-ICDD 38-1436) composition phases are noted in the case of 1073 K calcined sample.

At lower calcination temperatures, the particle size is normally small, and the surface area is large (Table 1). Hence the surface energy makes a large contribution to the total energy of the
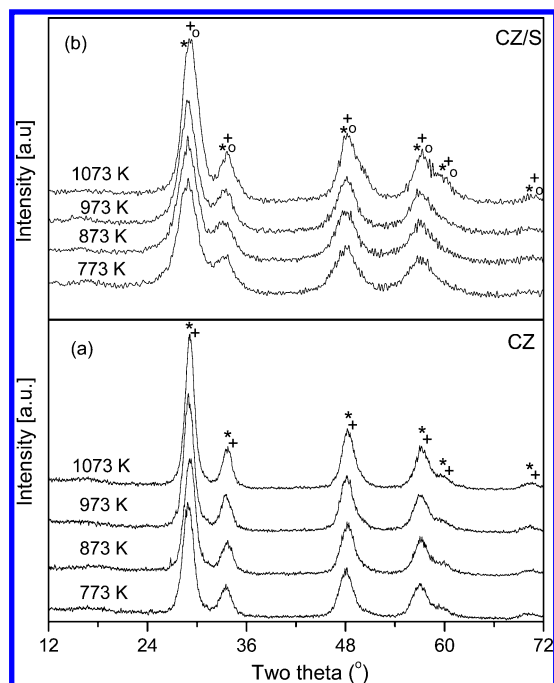
Figure 2. Powder X-ray diffraction (XRD) patterns of various $Ce_xZr_{1-x}O_2$ (CZ) and $Ce_xZr_{1-x}O_2/SiO_2$ (CZS) samples calcined at different temperatures. Peak legends are as follows: (*) lines due to $Ce_{0.75}Zr_{0.25}O_2$, (+) lines due to $Ce_{0.6}Zr_{0.4}O_2$, and ($\bigcirc$) lines due to $Ce_{0.5}Zr_{0.5}O_2$.

system. In this state the $Ce_{0.75}Zr_{0.25}O_2$ solid solution is thermodynamically metastable. As sintering proceeds and surface area decreases, the surface energy contribution becomes smaller and could explain the evolution of phases observed in the present investigation. Recently, Kenevey et al.,[32] reported the phase segregation phenomenon, which is considered to be surface-energy-driven, the solid solutions being stable as long as the crystallite size does not exceed a critical size, above which the surface energy contribution to the total energy of the system is too small to allow its stabilization thereby leading to the phase segregation. Within the detection limits of the XRD technique, there is no evidence about the presence of t-ZrO_2 or m-ZrO_2 phases in either of the investigated systems. Additionally, in the case of CZ/S samples the XRD features of silica are not apparent, indicating amorphous nature of the support. Another interesting observation to be mentioned from XRD measurements is that there are no extra lines due to compounds or mixed phases between CeO_2-SiO_2 and ZrO_2-SiO_2. However, formation of definite compounds between ceria-silica namely $Ce_{9.33}(SiO_4)_6O_2$ and zirconia−silica; namely, $ZrSiO_4$ is a well-established fact in the literature.[33,34] The nonappearance of these compounds could be attributed to a different preparation method adopted and lower calcination temperature employed in the present investigation.

Using the most intense line (111) of the $Ce_{0.75}Zr_{0.25}O_2$ pattern, cubic indexation and calculation of cell parameters have been carried out.[23,29] The evolution of *a* cell parameter for both CZ and CZ/S samples as a function of calcination temperature is shown in Table 1. It is evident from Table 1 that the size of the unit cell decreases gradually with increasing calcination temperature in agreement with Vegard's law,[35,36] which states that the lattice parameter of a solid solution is directly proportional to the atomic percent solute present.[37] Zirconium is reported to have an atomic radius ratio (r_{cation}/r_{anion}) of 0.59 compared to 0.68 for cerium.[38] This implies that zirconium has a smaller ionic radius and would result in a reduction of the lattice

parameter of the crystalline system when Ce^{4+} ions are substituted by Zr^{4+} ions. The calculated cubic lattice parameters (Table 1) are in consistent with these arguments.

The average crystallite sizes (D_{XRD}) of $Ce_xZr_{1-x}O_2$ phases in CZ and CZ/S samples as a function of calcination temperature are summarized in Table 1. It appears from Table 1 that crystallization of $Ce_xZr_{1-x}O_2$ solid solutions primarily depends on the calcination temperature as well as on the presence of SiO_2. An increase in the crystallite size is observed with increasing calcination temperature for both the series of samples and that the increase being slightly more for unsupported CZ samples. On the whole, the increase in the crystallite growth is very meager in both cases. It should be mentioned here that the particle size estimates of Ce−Zr−oxide solid solutions are subject to uncertainties due to compositional nonuniformity. When using the Scherrer equation, one assumes that the particle size effects are the only source of peak broadening. However, if compositional nonuniformity occurs in the particles, the particle size will be underestimated. As reported earlier, the origin of solid solutions between ceria and zirconia retards crystallite growth thus paving way for the formation of thermodynamically more stable phases.[39] In the case of CZ/S samples, it is expected that SiO_2 support stabilizes the Ce−Zr−oxide nanoparticles over its surface and inhibits the coagulation or grain growth (sintering) of the particles. There are certain advantages associated with the use of colloidal silica dispersions. First fact is that the colloidal dispersions are much less reactive toward the deposited catalytic materials, and, as a consequence, solid-state reactions are less likely to occur with the colloidal materials than with the coprecipitated materials from the soluble salts. Second, the particles of the colloids are larger than the particles of the coprecipitated salts. This has a feature of making larger pores and more open structures for the final catalyst. Thus the coprecipitation of ceria−zirconia along with colloidal silica yields smaller crystallites of Ce−Zr−oxides on the surface of the SiO_2. These crystallites, however, could coalesce under the impact of calcination thus accounting for a marginal increase in the crystallite size with increasing calcination temperature.

In contrast to XRD results, which yield information related to cation sublattice, Raman spectroscopy of the fluorite-type oxide structures are dominated by oxygen lattice vibrations, which are sensitive to the crystal symmetry, being thus a potential tool to obtain additional structural information.[40] The Raman spectra of CZ and CZ/S samples calcined at various temperatures are collected in Figure 3a,b. On the whole the Raman spectra of both series of samples are very similar. As presented in Figure 3a, the Raman spectrum of the CZ sample calcined at 773 K is dominated by a strong band at $\sim$470 cm^{-1} and a less prominent broad band at $\sim$600 cm^{-1}. The band at $\sim$470 cm^{-1} can be attributed to the F_{2g} Raman active mode of the fluorite type lattice. It can be viewed as a symmetric breathing mode of the oxygen atoms around cerium ions.[41] The Raman spectrum of CZ/S sample (Figure 3b) calcined at 773 K exhibits a strong band at $\sim$464 cm^{-1} along with a broad hump at $\sim$600 cm^{-1}. The band at $\sim$464 cm^{-1} is due to symmetric O−Ce−O stretching mode as mentioned earlier. According to literature, six Raman active modes ($A_{1g}+3E_g+2B_{1g}$) are expected for t-ZrO_2 (space group $P4_2/nmc$) while for the cubic fluorite structure of ceria (space group $Fm3m$) only one mode is Raman active.[42] No Raman lines due to ZrO_2 could be observed in either of the series of samples, thus corroborating with XRD results. As observed from Figure 3a,b, the relative intensity of the F_{2g} band increases with increasing calcination
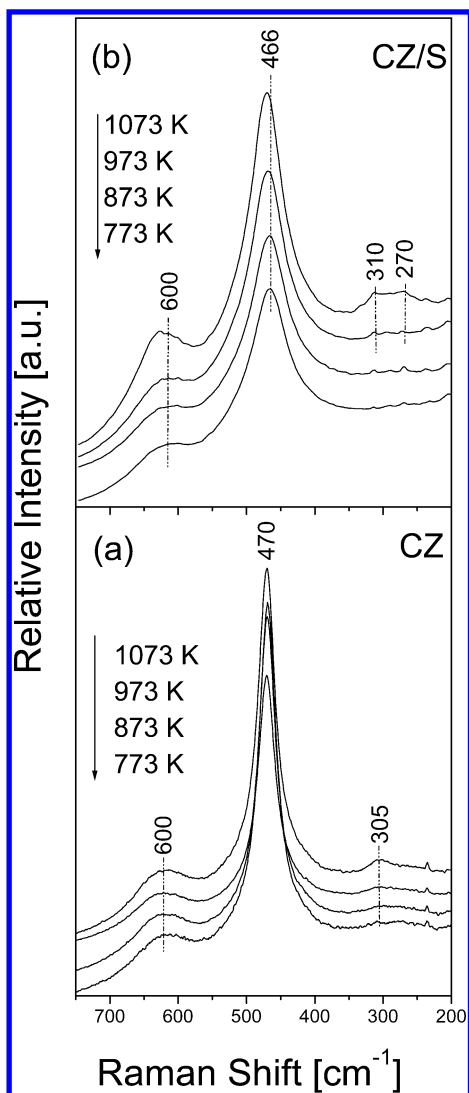
Figure 3. Raman spectra of Ce$_x$Zr$_{1-x}$O$_2$ (CZ) and Ce$_x$Zr$_{1-x}$O$_2$/SiO$_2$ (CZS) samples calcined at different temperatures.

Figure 4. TEM image of Ce$_x$Zr$_{1-x}$O$_2$ sample calcined at 773 K.

temperature that could be due to better crystallization of ceria−zirconia solid solutions at higher calcination temperatures. The shift in the Raman frequency to higher wavenumbers could be due to an increase in the zirconium content in the ceria-zirconia solid solution as evidenced by XRD results. The band shift observed in the case of CZ samples is very meager ($\sim$1 cm^{-1}), when compared to that of CZ/S samples (6 cm^{-1}). The higher shift of $\sim$6 cm^{-1} observed in the case of CZ/S sample calcined at 1073 K clearly accounts for the formation of Ce$_{0.6}$Zr$_{0.4}$O$_2$ phase.

On the whole the Raman bands of CZ/S are broader than CZ samples. The broadness of Raman peaks in the case of CZ/S samples could be attributed to the presence of SiO$_2$ support. It should be mentioned here that the intensity of the Raman band depends on several factors including grain size and morphology.[43] It is also known from literature that sintering of samples under high-temperature conditions leads to the formation of oxygen vacancies, which perturb the local M−O bond symmetry leading to the relaxation of symmetry selection rules.[41] The presence of a weak and less prominent broad band at $\sim$600 cm^{-1} can be attributed to a nondegenerate Raman inactive LO mode of ceria which arises due to relaxation of symmetry rules as stated above.[41,44] In particular, the substitution of zirconium into the ceria lattice with an increase in calcination temperature gives rise to oxygen vacancies, which are responsible for the
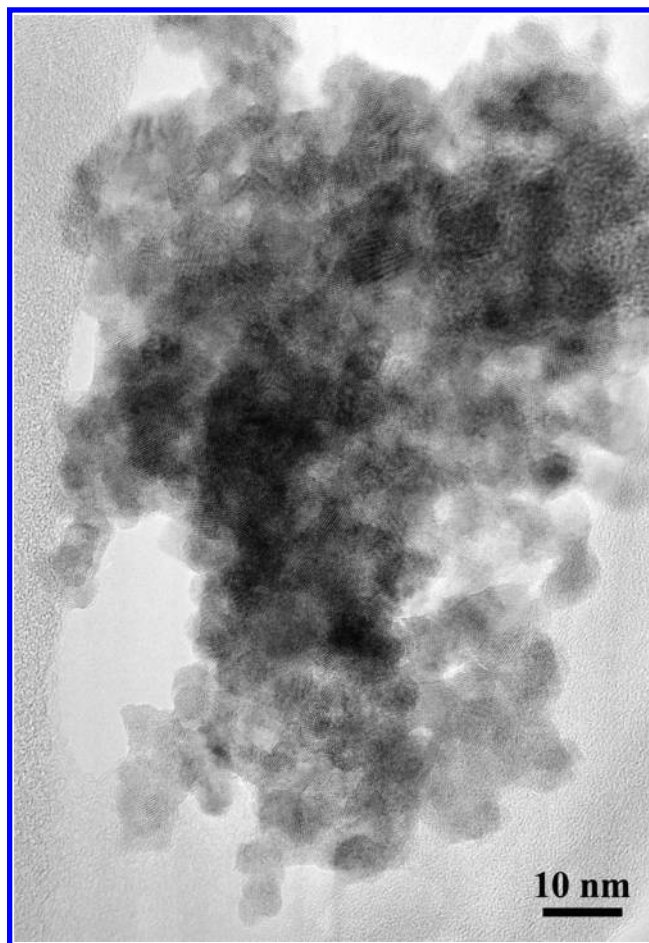
emergence of this band.[45] The appearance of weak bands at $\sim$300 cm^{-1}, at the calcination temperature of 1073 K, can be attributed to displacement of the oxygen atoms from their ideal fluorite lattice positions.[42] It is apparent from the Raman results that Ce$_x$Zr$_{1-x}$O$_2$ phases are mostly in cubic form in both cases and do not show any signs of tetragonal modification. For each sample, the spectra were recorded at several points and no shift in the band position or difference of width was noted. This observation reveals clearly that both CZ and CZ/S samples are homogeneous. In the case of CZ/S samples, silica did not show any Raman features, as reported in the literature.[46] This gives an impression that silica forms part of the substrate support on which ceria-zirconia solid solutions are dispersed. It is expected since the method of preparation adopted in the present study could result such a material. The absence of any other Raman features provides one more inference that silica is not forming any compound with cerium oxide, and zirconium oxide in line with XRD measurements.

To ascertain the results obtained from XRD and RS measurements and to explore the structural evolution at atomic scale, conventional TEM and HREM studies were performed on some selected representative samples. Representative TEM images of the Ce$_x$Zr$_{1-x}$O$_2$ sample calcined at 773 and 1073 K are shown in Figures 4 and 5, respectively. Analyses of these and other micrographs (not shown) reveal that the grain size increased from 5 to $\sim$10 nm with increasing calcination temperature from 773 to 1073 K. A representative HREM image of the sample calcined at 773 K and the digital diffraction pattern (DDP) corresponding to an individual particle of the image are shown in Figure 6. Similar HREM images were observed for the sample calcined at 1073 K. The inter planar spacing values of 3.0, 2.6,
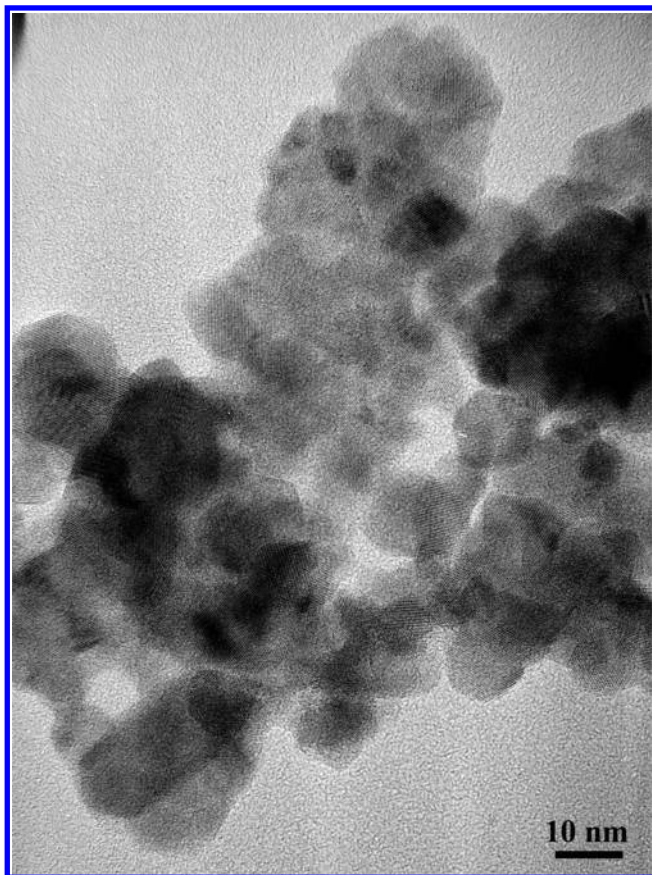
13550 *J. Phys. Chem. B, Vol. 109, No. 28, 2005*

Reddy et al.

Figure 5. TEM image of $Ce_xZr_{1-x}O_2$ sample calcined at 1073 K.

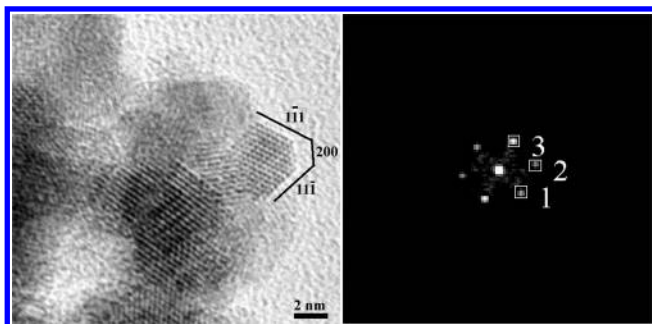**Figure 6.** HREM image of $Ce_xZr_{1-x}O_2$ sample calcined at 773 K and corresponding digital diffraction pattern (DDP).

Figure 7. TEM image of $Ce_xZr_{1-x}O_2/SiO_2$ sample calcined at 773 K along with corresponding SAED pattern.

Figure 8. TEM images of $Ce_xZr_{1-x}O_2/SiO_2$ sample calcined at 1073 K along with corresponding SAED pattern.

and 3.0 Å measured for the spots labeled 1, 2, and 3 (Figure 6) could be respectively assigned to (11-1), (200), and (1-11) family planes of the cubic structure, and the geometry of the DDP corresponds to the [011] zone axis. As per previous literature reports,[47,48] the electron diffraction pattern of fluorite cubic structure is characterized by the presence of first three electron diffraction rings which correspond to the inter planar spacings of ca. 3.1 (111), 2.7 (200), and 1.9 (220) Å. The other two likely phases, tetragonal and monoclinic, exhibit electron diffraction rings at or very close to these cubic spacings, as well as additional reflections. The additional spacings for the tetragonal phase are at 2.1 and possibly at 2.3, 3.7, and 5.3 Å (the last three being possibly active kinetic extinctions) and for the monoclinic at 2.0−2.3, 3.7, and 5.1 Å. These spacings should be treated as approximate since they will vary slightly with the Zr content of the sample. For example, the spots at 5.3 and 5.1 Å would be difficult to separate unambiguously. The absence of any of these additional spacings clearly indicates that the Ce−Zr−oxide system exists in the cubic modification. Taking
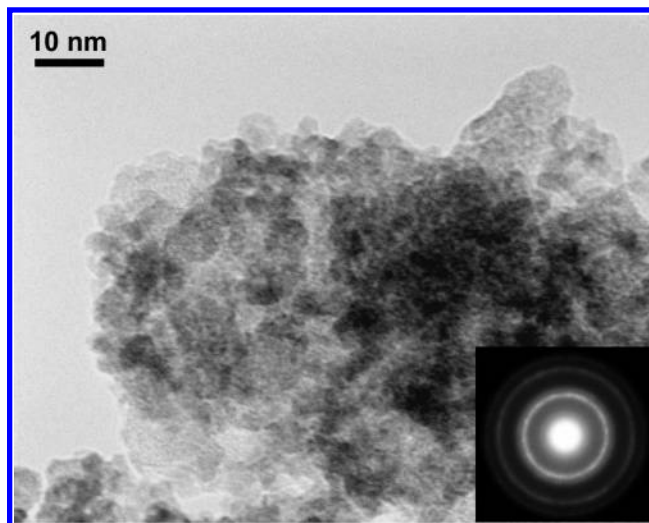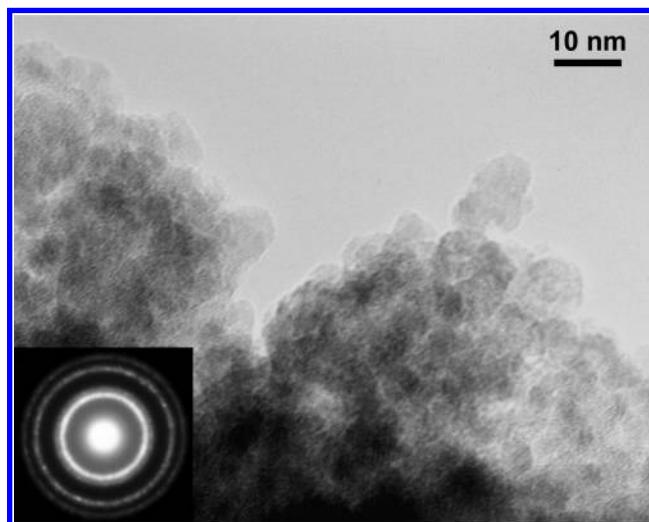
into account the slight contraction of crystal lattice expected by a partial substitution of Ce^{4+} ions by smaller Zr^{4+} ions, the simple fluorite type DDPs are quite obvious.[47,49] On the whole the $Ce_xZr_{1-x}O_2$ sample exhibits patterns of cubic only structures.

TEM global pictures of the CZ/S sample calcined at 773 and 1073 K along with their corresponding selected area diffraction patterns (SAED) are shown in Figures 7 and 8, respectively. A closer inspection of the images reveals the existence of small crystals (∼5 nm) dispersed over an amorphous matrix with different lighter contrasts. In both cases the broadening of the rings in the electron diffraction patterns account for the presence of such small randomly oriented mixed oxide particles. The position of these reflections, as in the case of unsupported samples, points out the existence of almost exclusively cubic structure. Figures 9 and 10 show HREM images of the CZ/S sample subjected to 773 and 1073 K, respectively. Well-dispersed very small Ce−Zr−oxide particles over the surface of the amorphous silica are mainly observed. Even after 1073 K calcination treatment, there was no apparent increase in the size of Ce−Zr−oxide particles. These conclusions are postulated both from the observation of the experimental images and the analysis of the selected area electron diffraction patterns. The fringes that appear in the micrograph allow for the identification of the crystallographic spacings of the $Ce_xZr_{1-x}O_2$ nanocrys-

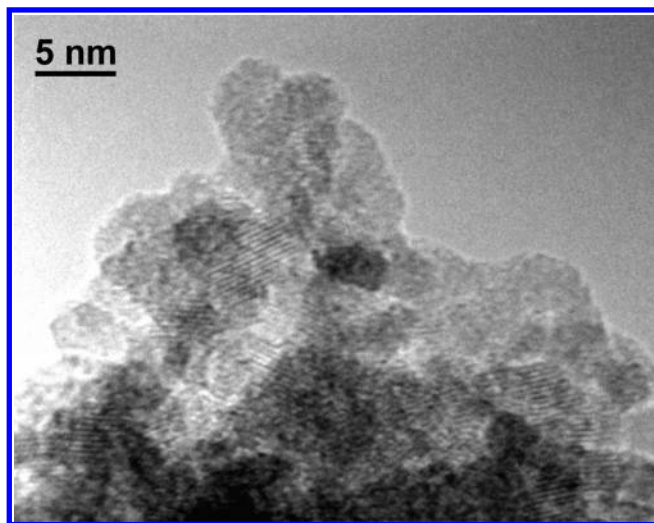**Figure 9.** HREM image of Ce$_x$Zr$_{1-x}$O$_2$/SiO$_2$ sample calcined at 773 K.
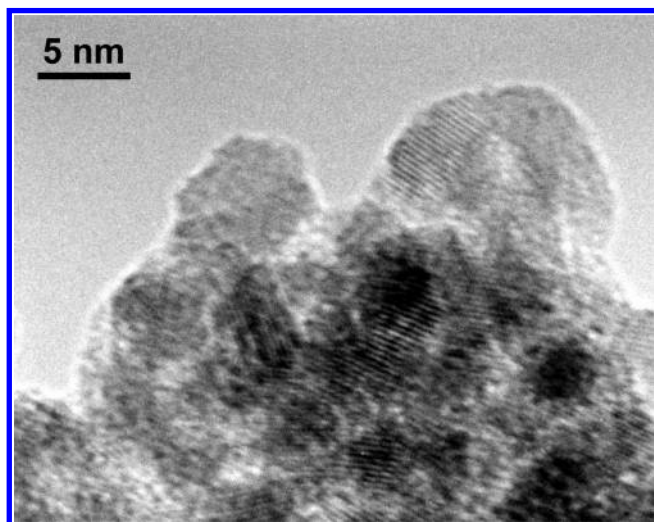

Figure 10. HREM image of Ce$_x$Zr$_{1-x}$O$_2$/SiO$_2$ sample calcined at 1073 K.

TABLE 2: Percentage Weight Loss (%) and Corresponding Oxygen Vacancy Concentration δ in Unsupported and Silica Supported CeO$_2$-ZrO$_2$ Samples as Determined by Thermogravimetry

sample[a]	weight loss (%)	δ
CeO$_2$-ZrO$_2$	0.11	0.035
CeO$_2$-ZrO$_2$/SiO$_2$	0.27	0.086

a Calcined at 773 K.

tallites. Lattice fringes of around 3 Å are extensively observed on very small well-dispersed particles supported on the amorphous contrast of silica. Thus the combined XRD, Raman, and HREM studies provide valuable information on the structural evolution of the unsupported and silica supported CeO$_2$−ZrO$_2$ mixed oxide catalysts.

The potential OSC of 773 K calcined CZ and CZ/S samples were evaluated by thermogravimetry. The percentage weight loss (%) and the corresponding oxygen vacancy concentration or storage capacity (δ) are presented in Table 2. The parameter δ denotes the number of oxygen vacancies formed in the given sample under the given set of experimental conditions employed. As can be noted from Table 2, there is a substantial enhancement in the OSC of CZ/S sample when compared to that of unsupported CZ (same amount of sample). Since SiO$_2$ was

found to show no OSC property under the experimental conditions employed in this study, it can be stated that a highly dispersed and stabilized nanosized Ce$_x$Zr$_{1-x}$O$_2$ oxides over the high surface area silica, in line with XRD and HREM results, are responsible for the enhancement in the OSC of the sample. A comparison of the results with other systems from the literature reveals that the silica supported Ce$_x$Zr$_{1-x}$O$_2$ exhibits reasonably good OSC properties.[50] As per literature reports, nanocrystalline ceria has a lower energy of reduction compared to bulk ceria and is known to be responsible for higher defect population.[1] By supporting the Ce$_x$Zr$_{1-x}$O$_2$ over the silica, the undesirable deactivation due to sintering of the nanosized oxides could be minimized thereby leading to the thermally stable OSC systems. In summary, materials, which are highly suitable for thermally demanding redox reactions, such as those mediated by TWCs, can be obtained by supporting Ce$_x$Zr$_{1-x}$O$_2$ mixed oxides over the silica. Further work is under active progress to exploit these supported nanosized oxides for technologically important catalytic reactions.

Conclusions

(1) By adopting a deposition precipitation method, preparation of highly dispersed nanocrystalline Ce$_x$Zr$_{1-x}$O$_2$ (1:1 mole ratio) solid solutions over the surface of SiO$_2$ was undertaken. Unsupported nanocrystalline Ce$_x$Zr$_{1-x}$O$_2$ was also synthesized by a coprecipitation method for the purpose of comparison. To evaluate temperature stability, these oxides were subjected to thermal treatments from 773 to 1073 K and were examined by using XRD, Raman, and HREM techniques. The influence of SiO$_2$ support on the structure of Ce$_x$Zr$_{1-x}$O$_2$ and its temperature stability was mainly contemplated. (2) The XRD measurements revealed the formation of Ce$_{0.75}$Zr$_{0.25}$O$_2$ and Ce$_{0.6}$Zr$_{0.4}$O$_2$ phases in the case of CZ sample, and Ce$_{0.75}$Zr$_{0.25}$O$_2$, Ce$_{0.6}$Zr$_{0.4}$O$_2$, and Ce$_{0.5}$Zr$_{0.5}$O$_2$ in different proportions in the case of CZ/S sample. The crystallinity and the formation of zirconia rich phases increased with increasing calcination temperature. (3) The cell *a* parameter estimations from XRD measurements indicated contraction of the ceria lattice with increasing calcination temperature due to incorporation of Zr^{4+} into the ceria unit cell. (4) Raman measurements establish generally the fluorite structure of Ce$_x$Zr$_{1-x}$O$_2$ and indicate the presence of oxygen vacancies/Ce^{3+}, lattice defects, and displacement of oxygen ions from their normal lattice positions in both the series of samples. (5) The HREM results revealed, in case of CZ/S samples, a well-dispersed nanosized Ce−Zr-oxides over the surface of amorphous SiO$_2$. The size of these supported mixed oxide particles is very small ($\sim$5 nm) even after 1073 K treatment. However, the crystallite size increased from 5 to $\sim$10 nm with increasing calcination temperature in the case of CZ samples. The precise structural features of Ce$_x$Zr$_{1-x}$O$_2$ nanocrystals as determined by digital diffraction analysis of the HREM experimental images revealed that these are mainly in the cubic fluorite geometry. (6) The CZ/S sample exhibits more oxygen storage capacity than CZ sample due to highly dispersed nanosized Ce$_{1-x}$Zr$_x$O$_2$ oxides over the surface of silica.

References and Notes

(1) Monte, R. Di; Kaspar, J. *J. Mater. Chem.* **2005**, *15*, 633 and references therein.
(2) Daturi, M.; Finocchio, E.; Binet, C.; Lavalley, J. C.; Fally. F.; Perrichon, V. *J. Phys. Chem. B* **1999**, *103*, 4884.

(3) Gandhi, H. S.; Graham, G. W.; McCabe, R. W. *J. Catal.* **2003**, *216*, 433 and references therein.

(4) Trovarelli, A.; de Leitenburg, C.; Dolcetti, G. *Chem. Tech*. **1997**, *27*, 32.

(5) Bernal, S.; Kaspar, J.; Trovarelli, A.; Eds. Recent Progress in Catalysis by Ceria and Related Compounds, *Catal. Today* **1999**, *50*, 173.

(6) Martinez-Ariaz, A.; Fernandez-Garcia, M.; Iglesias Juez, A.; Hungria, A. B.; Anderson, J. A.; Conesa, J. C.; Soria, J. *Appl. Catal. B: Environ.* **2001**, *31*, 51.

(7) Sadykov, V. A.; Snegurenko, O. I.; Rogov, V. A.; Zolotarskii, I. A.; Moroz, E. M. *Catal. Today* **2004**, *91−92*, 299.

(8) Noronha, F. B.; Fendley, E. C.; Soares. R. R.; Alvarez. W. E.; Resasco. D. E. *Chem. Eng. J.* **2001**, *82*, 21.

(9) Terribile, D.; Trovarelli. A.; de Leitenburg, C.; Primavera, A.; Dolcetti, G. *Catal. Today* **1999**, *47*, 133.

(10) Liu, Y.; Hayakawa, T.; Ishii, T.; Kumagai, M.; Yasuda, H.; Suzuki, K.; Hamakawa, S.; Marata, K. *Appl. Catal. A: Gen*. **2001**, *210*, 301.

(11) Srinivas, D.; Satyanarayana, C. V. V.; Potdar, H. S.; Ratnasamy, P. *Appl. Catal. A: Gen.* **2003**, *246*, 323.

(12) Solinas, V.; Rombi, E.; Ferino, I.; Cutrufello, M. G.; Colon, G.; Navio, J. A. *J. Mol. Catal : A: Chem*. **2003**, *204−205*, 629.

(13) Pengpanich, S.; Meeyoo, V.; Rirksomboon, T.; Bunyakiat, K. *Appl. Catal. A: Gen.* **2002**, *234*, 221.

(14) Bozo, C.; Guilhaume, N.; Garbowski, E.; Primet, M. *Catal. Today* **2000**, *59,* 33.

(15) Thammachart, M.; Meeyoo, V.; Risksomboon, T.; Osuwan, S. *Catal. Today* **2001**, *68*, 53.

(16) Boaro, M.; de Leitenburg, C.; Dolcetti, G.; Trovarelli, A. *J. Catal.* **2000**, *193*, 338.

(17) Martinez Arias, A.; Fernandez-Garcia, M.; Hungria, A. B.; Iglesias-Juez, A.; Galvez, O.; Anderson, J. A.; Conesa, J. C.; Soria, J.; Munuera, G. *J. Catal.* **2003**, *214*, 261.

(18) Wootsch, A.; Descorme, C.; Duprez, D. *J. Catal*. **2004**, *225*, 259.

(19) Ratnasamy, P.; Srinivas, D.; Satyanarayana, C. V. V.; Manikandan, P.; Senthil Kumaran, R. S.; Sachin, M.; Vasudev N. Shetti. *J. Catal.* **2004**, *221*, 455.

(20) Breen, J. P.; Burch, R.; Coleman, H. M. *Appl. Catal. B: Environ.* **2002**, *39*, 65.

(21) Kaspar, J.; Fornasiero, P.; Graziani, M. *Catal. Today* **1999**, *50*, 285.

(22) Trovarelli, A. *Catal. Rev. Sci. Eng*. **1996**, *38*, 439.

(23) Bozo, C.; Gaillard, F.; Guilhaume, N. *Appl. Catal*. *A: Gen.* **2001**, *220*, 69.

(24) Si, R.; Zhang, Y.-W.; Li, S.-J.; Lin, B.-X.; Yan, C.-H. *J. Phys. Chem. B* **2004**, *108*, 12481.

(25) Monte, R. Di.; Fornasiero, P.; Kaspar, J.; Graziani, M.; Gatica, J. M.; Bernal, S.; Gómez Herreroc, A. *Chem. Commun.* **2000**, 2167.

(26) Monte, R. Di.; Fornasiero, P.; Desinan, S.; Kaspar, J.; Gatica, J. M.; Calvino, J. J.; Fonda, E. *Chem. Mater.* **2004**, *16*, 4273.

(27) Reddy, B. M.; Khan, A.; Lakshmanan, P.; Aouine, M.; Loridant, S.; Volta, J. C. *J. Phys. Chem. B* **2005**, *109*, 3355.

(28) Sugiura, M. *Catalysis Surveys from Asia* **2003**, *7*, 77.

(29) Colón, G.; Pijolat, M.; Valdivieso, F.; Vidal, H.; Kaspar, J.; Daturi, M.; Finocchio, E.; Binet, C.; Lavalley, J. C.; Baker, R. T.; Bernal, S. *J. Chem. Soc., Faraday Trans.* **1998**, *94*, 3717.

(30) Ozawa, M.; Loong, C. K. *Catal. Today* **1999**, *50*, 329.

(31) Logan, A. D.; Shelef, M. *J. Mater. Res.* **1994**, *9*, 468.

(32) Kenevey, K.; Valdivieso, F.; Soustelle, M.; Pijolat, M. *Appl. Catal. B: Environ.* **2001**, *29*, 93

(33) Rocchini, E.; Trovarelli, A.; Liorca, J.; Graham, G. W.; Weber, W. H.; Maciejewski, M.; Baiker, A. *J. Catal.* **2000**, *194*, 461.

(34) Kucharczyk, B.; Tylus, W.; Kepinski, L. *Appl. Catal. B: Environ.* **2004**, *49,* 27.

(35) Shannon, R. D. *Acta Crystallogr*. **1976**, *A32*, 751.

(36) Meriani, S.; Spinolo, G. *Powder Diffract*. **1987**, *2*, 255.

(37) Cullity, B. D. Elements of X-ray Diffraction, Addison-Wesley: Reading, MA, 1956.

(38) Ingel, R. P.; Lewis, P.; Bender, B. A.; Rice, R. W. *Adv. Ceram*. **1984**, *12*, 408.

(39) Reddy, B. M.; Khan, A.; Yamada, Y.; Kobayashi, T.; Loridant, S.; Volta, J. C. *Langmuir* **2003**, *19*, 3025.

(40) Knözinger, H.; Mestl, G. *Top. Catal.* **1999**, *8*, 45.

(41) Lin, X.-M.; Li, L.-P.; Li, G.-S.; Su, W.-H. *Mater. Chem. Phys*. **2001**, *69*, 236.

(42) Yashima, M.; Arashi, H.; Kakihana, M.; Yoshimura, M. *J. Am. Ceram. Soc.* **1994**, *77*, 1067.

(43) Spanier, J. E.; Robinson, R. D.; Zhang, F.; Chan, S. W.; Herman, I. P. *Phys. Rev. B* **2001**, *64*, 245407.

(44) Weber, W. H.; Hass, K. C.; McBride, J. R.; *Phys. Rev. B* **1993**, *48*, 178.

(45) McBride, J. R.; Hass, K. C.; Poindexter, B. D.; Weber, W. H. *J. Appl. Phys.* **1994**, *76*, 2435.

(46) Wachs, I. E.; Deo, G. *J. Phys. Chem.* **1991**, *95*, 5889.

(47) Colon, G.; Pijolat, M.; Valdivieso, F.; Vidal, H.; Kaspar, J.; Finocchio, E.; Daturi, M.; Binet, C.; Lavalley, J. C.; Baker, R. T.; Bernal, S. *J. Chem. Soc., Faraday Trans*. **1998**, *94*, 3717.

(48) Colon, G.; Valdivieso, F.; Pijolat, M.; Baker, R. T.; Calvino, J. J.; Bernal, S. *Catal. Today* **1999**, *50*, 271.

(49) Reddy, B. M.; Khan, A.; Yamada, Y.; Kobayashi, T.; Loridant, S.; Volta, J. C. *J. Phys. Chem. B* **2003**, *107*, 11475.

(50) Ozawa, M.; Matuda, K.; Suzuki, S. *J. Alloys Compd.* **2000**, *303−304*, 56.